


Magic angle butterfly in twisted trilayer graphene

Fedor K. Popov  and Grigory Tarnopolsky

*Department of Physics, New York University, New York, New York 10003, USA
and Department of Physics, Carnegie Mellon University, Pittsburgh, Pennsylvania 15213, USA*



(Received 13 June 2023; accepted 19 September 2023; published 24 October 2023)

We consider a configuration of three stacked graphene monolayers with commensurate twist angles $\theta_{12}/\theta_{23} = p/q$, where p and q are coprime integers with $0 < p < |q|$ and q can be positive or negative. We study this system using the continuum model in the chiral limit when interlayer coupling terms between AA₁₂ and AA₂₃ sites of the moiré patterns 12 and 23 are neglected. There are only three inequivalent displacements between the moiré patterns 12 and 23, at which the three monolayers' Dirac zero modes are protected. Remarkably, for these displacements and an arbitrary p/q we discover exactly flat bands at an infinite set of twist angles (magic angles). We provide theoretical explanation and classification of all possible configurations and topologies of the flat bands.

DOI: [10.1103/PhysRevResearch.5.043079](https://doi.org/10.1103/PhysRevResearch.5.043079)

I. INTRODUCTION AND SUMMARY

Two graphene layers placed one on top of the other with a relative small twist angle form a periodic moiré pattern, which alters significantly the low-energy electronic spectrum. At the special twist “magic” angle $\theta_* \approx 1.05^\circ$ a dramatic flattening of the lowest energy bands was observed in [1,2]. These almost dispersionless electronic bands hinted to a possibility of interesting strongly interacting phenomena, which was subsequently confirmed through a series of experimental studies [3–5]. These tantalizing experiments have inspired numerous theoretical and experimental investigations [6–34], and the field continues to advance with fascinating new proposals and insights.

Multiple layers of graphene stacked on top of each other with small relative twist angles [35–48] provide even greater versatility compared to twisted bilayer graphene (TBG) due to the increased number of parameters. Initial theoretical investigations of alternating-twist trilayer graphene (aTTG) [35] demonstrated a similar flattening of electronic bands at “magic” angles, ultimately leading to the experimental discovery of various correlated phenomena [49–54] at the angles predicted in [35]. The study of the interaction effects in such systems remains an active area of ongoing theoretical investigations [55–57].

In [36,39] a general configuration of twisted trilayer graphene was proposed, where the three layers are consecutively twisted by small angles $\theta_{12} = p\theta$ and $\theta_{23} = q\theta$, where p and q are coprime integers $0 < p < q$, as shown in Fig. 1. The analysis of electronic bands in this system, was initially performed using the continuum model with equal

interlayer coupling terms between AA and AB sites of the moiré patterns. However, this model did not exhibit a distinct phenomenon of band flattening.

The existence of magic angles and perfectly flat bands was recently discovered in the case of equal-twist trilayer graphene (eTTG) [58], where the twist angles between layers 1 and 2 (θ_{12}) and between layers 2 and 3 (θ_{23}) are equal. The chiral limit of the twisted graphene continuum model [29,30,59] was crucial in revealing these magic angles and flat bands. In this limit, the interlayer coupling terms between AA sites in the moiré pattern are disregarded, resulting in the Hamiltonian exhibiting exactly flat bands at an infinite series of magic angles.

In addition to the twist angles, the spectrum of a general twisted trilayer graphene (TTG) system is influenced by the relative displacement \mathbf{d} between the two moiré patterns formed by layers 12 and 23 [39]. The investigation of equal-twist trilayer graphene (eTTG) without any displacement between the moiré patterns ($\mathbf{d} = 0$, AAA stacking) revealed an intriguing connection between the flat bands of twisted bilayer graphene and eTTG, establishing a relation between the magic angles in these distinct systems. A subsequent study by Guerzi *et al.* [60] (see also [61,62]) demonstrated that eTTG system exhibits a “moiré of moiré” pattern, resulting in large triangular regions of ABA and BAB stacking [$\mathbf{d} = \pm \frac{1}{3}(\mathbf{a}_1 - \mathbf{a}_2)$, where $\mathbf{a}_{1,2}$ are the single moiré lattice unit vectors] separated by smaller AAA regions. By employing the chiral model with ABA or BAB stacking of the graphene layers, another set of magic angles and perfectly flat bands were unveiled. Furthermore, it was shown that the flat bands in eTTG can possess the Chern number $C = 2$, and the mathematical origin of such flat bands was explained.

In this letter, we analyze the general twisted trilayer graphene configuration in which the consecutive layers are twisted at small but commensurate angles $\theta_{12} = p\theta$ and $\theta_{23} = q\theta$, where p and q are coprime integer numbers $0 < p < |q|$ and q can be positive or negative. We refer to

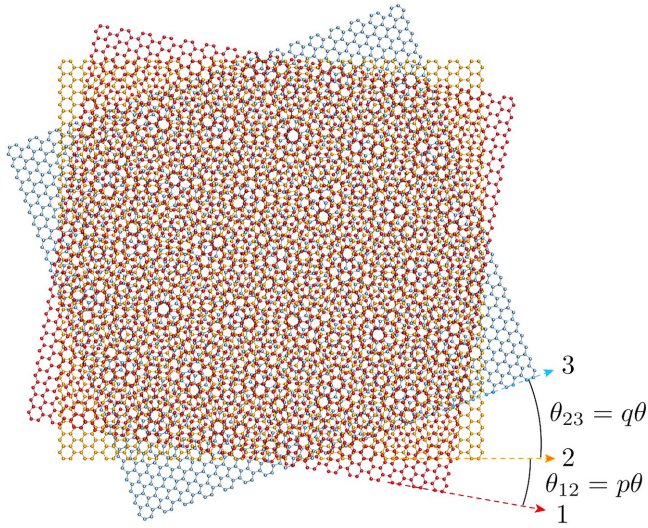


FIG. 1. Picture of a pq -twist trilayer graphene (pqTTG) with $(p, q) = (1, 2)$.

this system as pq -twist trilayer graphene (pqTTG), and it is schematically depicted in Fig. 1. Such configuration was recently achieved in an experiment [54]. We analyze the continuum model and take the chiral limit, where interlayer coupling terms are $w_{AB} \approx 110\text{meV}$ and $w_{AA} = 0$ (this limit is motivated by the lattice relaxation effects, which imply $w_{AA} < w_{AB}$ [63]).

For small twist angles we assume that the moiré patterns 12 and 23 are formed by vectors $p\mathbf{a}_{1,2}$ and $q\mathbf{a}_{1,2}$, where $\mathbf{a}_{1,2} = (4\pi/3k_\theta)(\pm\sqrt{3}/2, 1/2)$ with $k_\theta = 2k_D \sin(\theta/2) \approx k_D\theta$ and $k_D = 4\pi/3\sqrt{3}a$ is the Dirac momentum of the monolayer graphene with lattice constant $a \approx 1.42 \text{ \AA}$. Similarly to the previously discussed eTTG configuration, pqTTG also has a moiré of moiré pattern, resulting in local variations of the displacement vector \mathbf{d} between the moiré patterns 12 and 23. There are only three inequivalent displacement vectors, at which the three monolayers' Dirac zero modes are protected. These are $\mathbf{d} = 0$ and $\mathbf{d} = \pm\mathbf{d}_0$, where $\mathbf{d}_0 = \frac{1}{3p|q|}(\mathbf{a}_1 - \mathbf{a}_2)$ and the spectrum is invariant under the shifts $\mathbf{d} \rightarrow \mathbf{d} + \frac{1}{pq}\mathbf{a}_{1,2}$. The values of the magic angles are identical for the displacements $\pm\mathbf{d}_0$. Remarkably, in the chiral limit and these displacements the electronic energy spectrum exhibits perfectly flat bands at an infinite sequence of magic angles for any combination of coprime integers p and q . We introduce dimensionless twist parameters $\alpha_{12} = \alpha/p$ and $\alpha_{23} = \alpha/q$ where $\alpha = w_{AB}/(v_F k_D \theta)$, and $v_F \approx 10^6 \text{ m/s}$ is the monolayer graphene Fermi velocity (for brevity we also refer to α_{12} , α_{23} and α as twist angles). The twist angle could be recovered as $\theta \approx \frac{0.62^\circ}{\alpha}$. We plot magic angles α_{12} as a function of p/q in Fig. 2. Plot of the magic angles (α_{12} , α_{23}) for different p/q is shown in Fig. 3. Finally we present Tables I and II of the first four magic angles α_{12} for various values of p and q and displacements $\mathbf{d} = 0$ and $\mathbf{d} = \pm\mathbf{d}_0$.

Below we formulate the continuum model for twisted trilayer graphene, present the criteria for the emergence of perfectly flat bands and provide a complete classification of the structures of the flat bands at magic angles.

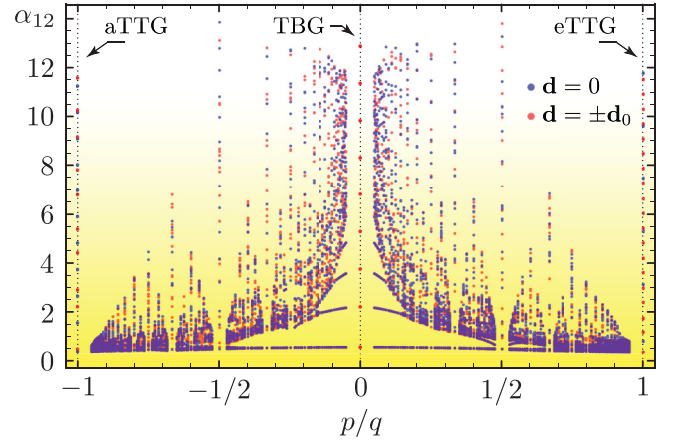


FIG. 2. The magic angle butterfly. Plot of the leading magic angles α_{12} for all possible ratios p/q of coprime integers p and q with $0 < p < |q|$ and up to $|q| = 20$ and displacements $\mathbf{d} = 0, \pm\mathbf{d}_0$. Near the center ($p/q = 0$) the magic angles approach those of TBG.

II. CONTINUUM MODEL FOR TWISTED TRILAYER GRAPHENE

We consider a system of three stacked graphene monolayers, where each layer $\ell = 1, 2, 3$ is rotated counterclockwise by an angle θ_ℓ around an atom site and then shifted by a vector \mathbf{d}_ℓ , so atoms in each layer are parametrized by $\mathbf{r} = R_{\theta_\ell}(\mathbf{R} + \tau_\alpha) + \mathbf{d}_\ell$, where $R_\theta = e^{-i\theta\sigma_y}$ is the rotation matrix and \mathbf{R} and τ_α run over the lattice and sublattice sites. The continuum model Hamiltonian for twisted trilayer graphene at the K valley can be written as [35]

$$H = \begin{pmatrix} -iv_F\sigma_{\theta_1}\nabla & T^{12}(\mathbf{r} - \mathbf{d}_{12}) & 0 \\ T^{12\dagger}(\mathbf{r} - \mathbf{d}_{12}) & -iv_F\sigma_{\theta_2}\nabla & T^{23}(\mathbf{r} - \mathbf{d}_{23}) \\ 0 & T^{23\dagger}(\mathbf{r} - \mathbf{d}_{23}) & -iv_F\sigma_{\theta_3}\nabla \end{pmatrix},$$

where $\sigma_\theta \equiv e^{i\frac{\theta}{2}\sigma_z}\sigma e^{-i\frac{\theta}{2}\sigma_z}$, $\sigma = (\sigma_x, \sigma_y)$, and $\mathbf{d}_{\ell\ell'} = \frac{1}{2}(\mathbf{d}_\ell + \mathbf{d}_{\ell'} + i \cot(\theta_{\ell\ell'}/2)\sigma_y(\mathbf{d}_\ell - \mathbf{d}_{\ell'}))$ is the moiré pattern displacement vector. The moiré potential between adjacent layers ℓ and ℓ' is

$$T^{\ell\ell'}(\mathbf{r}) = \sum_{n=1}^3 T_n^{\ell\ell'} e^{-i\mathbf{q}_n^{\ell\ell'} \cdot \mathbf{r}}, \quad (1)$$

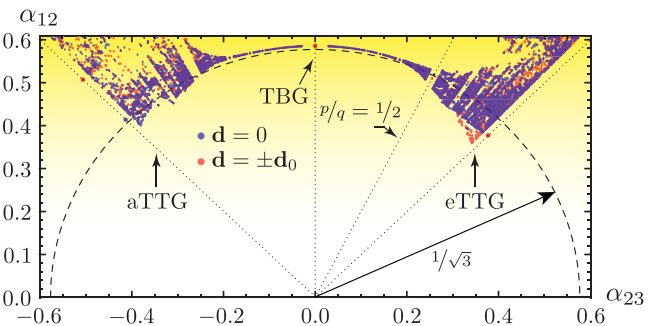


FIG. 3. Plot of the leading magic angles (α_{12} , α_{23}) for all possible ratios p/q of coprime integers p and q with $0 < p < |q|$ and up to $|q| = 20$. The black dashed line is a semicircle $\alpha_{12}^2 + \alpha_{23}^2 = 1/3$ derived in [38] using perturbation theory.

TABLE I. The table of magic angles for various $p, q > 0$.

$(p, q)_d$	$\alpha_{12}^{(1)}$	$\alpha_{12}^{(2)}$	$\alpha_{12}^{(3)}$	$\alpha_{12}^{(4)}$
$(1, 4)_0$	0.5673	1.4042	1.8253	1.8295
$(1, 4)_{\pm d_0}$	0.5672	1.6416 ₄	1.7963	2.0260 ₄
$(1, 3)_0$	0.5542	1.2025	2.8487	4.0074
$(1, 3)_{\pm d_0}$	0.5527	1.2464	1.3919	2.0304
$(1, 2)_0$	0.5194	0.9589	1.0255 ₄	1.5309 ₄
$(1, 2)_{\pm d_0}$	0.5094	1.0698	1.6226	2.9886
$(2, 3)_0$	0.4403	0.4549	0.4954 ₄	0.7662 ₄
$(2, 3)_{\pm d_0}$	0.4527	0.4548	0.4668	0.5010
$(3, 4)_0$	0.4356	0.4710	0.4941 ₄	0.5012
$(3, 4)_{\pm d_0}$	0.4269	0.4302	0.4612	0.4646
$(1, 1)_0$	0.8283 ₄	3.1412 ₄	5.3053 ₄	7.4621 ₄
$(1, 1)_{\pm d_0}$	0.3771	1.1967 ₄	1.7549	2.4136 ₄

where $T_{n+1}^{\ell\ell'} = w_{AA}^{\ell\ell'} \sigma_0 + w_{AB}^{\ell\ell'} (\sigma_x \cos n\phi + \sigma_y \sin n\phi)$ and

$$\mathbf{q}_1^{\ell\ell'} = 2k_D \sin(\theta_{\ell\ell'}/2) \mathbf{R}_{\phi_{\ell\ell'}}(0, -1), \quad \mathbf{q}_{2,3}^{\ell\ell'} = R_{\pm\phi} \mathbf{q}_1^{\ell\ell'} \quad (2)$$

with $\theta_{\ell\ell'} = \theta_\ell - \theta_{\ell'}$, $\phi_{\ell\ell'} = (\theta_\ell + \theta_{\ell'})/2$, $\phi = 2\pi/3$. The coupling between adjacent layers ℓ and ℓ' is characterized by two parameters $w_{AA}^{\ell\ell'}$ and $w_{AB}^{\ell\ell'}$ representing intra- and inter-sublattice couplings. The chiral limit corresponds to $w_{AA}^{\ell\ell'} = 0$. Also using translation invariance we can make a replacement $\mathbf{r} \rightarrow \mathbf{r} + \mathbf{d}_{12}$, and therefore the Hamiltonian depends only on a single displacement vector $\mathbf{d} = \mathbf{d}_{23} - \mathbf{d}_{12}$.

We consider a trilayer configuration where the relative twists are commensurate $\theta_{21} = p\theta$ and $\theta_{32} = q\theta$ and p and q are two coprime integers, which satisfy $0 < p < |q|$. For a small angle θ we can set $\phi_{1\ell'} = 0$ leading to $\mathbf{q}_1^{12} = p\mathbf{q}_1$ and $\mathbf{q}_1^{23} = q\mathbf{q}_1$ and $\mathbf{q}_1 = k_\theta(0, -1)$ with $k_\theta = 2k_D \sin(\theta/2) \approx k_D\theta$. Thus we obtain the following Hamiltonian:

$$H_{\text{pqTTG}} = \begin{pmatrix} -iv_F \sigma_{-p\theta} \nabla & T(p\mathbf{r}) & 0 \\ T^\dagger(p\mathbf{r}) & -iv_F \sigma \nabla & T(q(\mathbf{r} - \mathbf{d})) \\ 0 & T^\dagger(q(\mathbf{r} - \mathbf{d})) & -iv_F \sigma_{q\theta} \nabla \end{pmatrix}, \quad (3)$$

where we assume equal couplings between layers. For a small twist angle θ we can neglect the phase factors in the Pauli matrices $\sigma_{-p\theta} \rightarrow \sigma$ and $\sigma_{q\theta} \rightarrow \sigma$.

TABLE II. The table of magic angles for various $p, -q > 0$.

$(p, q)_d$	$\alpha_{12}^{(1)}$	$\alpha_{12}^{(2)}$	$\alpha_{12}^{(3)}$	$\alpha_{12}^{(4)}$
$(1, -1)_0$	0.4141	1.5706	2.6526	3.7310
$(1, -1)_{\pm d_0}$	0.5072	2.2295	2.9043	4.4080
$(3, -4)_0$	0.4821	0.4887 ₄	0.6493	0.6626 ₄
$(3, -4)_{\pm d_0}$	0.5121	0.6167	0.6520	0.6954
$(2, -3)_0$	0.4912 ₄	0.5054	1.2890	1.3259 ₄
$(2, -3)_{\pm d_0}$	0.9458	1.0945	1.7939	2.2357
$(1, -2)_0$	0.5131	1.5014	2.0490	3.2157
$(1, -2)_{\pm d_0}$	0.5857	0.7614	1.3797	1.8178 ₄
$(1, -3)_0$	0.5574	1.4373	2.6738 ₄	3.9906 ₄
$(1, -3)_{\pm d_0}$	0.5587	1.2915	1.3920	2.1730
$(1, -4)_0$	0.5685	1.7225 ₄	1.8548 ₄	3.2869
$(1, -4)_{\pm d_0}$	0.5685	1.7130	1.7298	1.9467

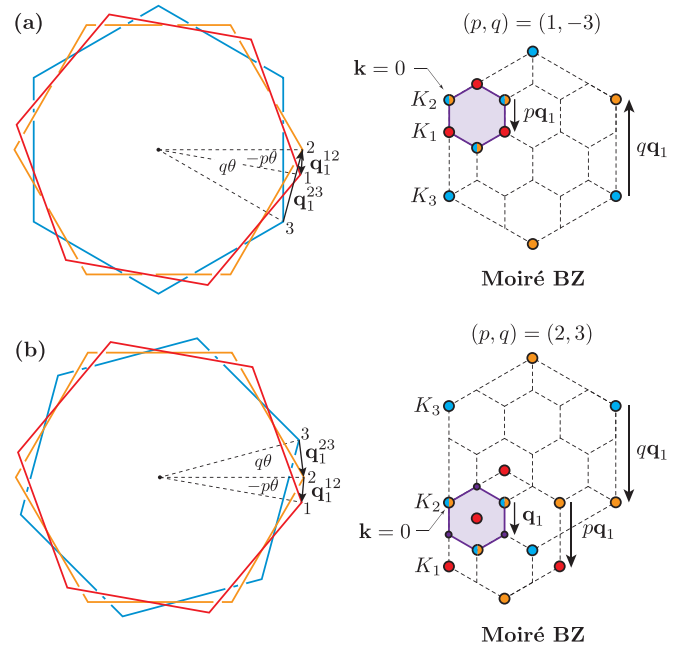


FIG. 4. Original Brillouin zones of three graphene layers with their Dirac points K_1, K_2 , and K_3 and the moiré Brillouin zones for pqTTG. The layers are twisted by the angles $p\theta$ and $q\theta$, where p and q are coprime integers such that $0 < p < |q|$. The wave vector \mathbf{k} is zero at the Dirac point K_2 . We neglect a relative rotation between vectors \mathbf{q}_1^{12} and \mathbf{q}_1^{23} and assume that $\mathbf{q}_1^{12} = p\mathbf{q}_1$ and $\mathbf{q}_1^{23} = q\mathbf{q}_1$. (a) Case $(p, q) = (1, -3)$. (b) Case $(p, q) = (2, 3)$.

The moiré Brillouin zone (mBZ) for this Hamiltonian is depicted in Fig. 4. The reciprocal moiré unit vectors are $\mathbf{b}_{1,2} = \mathbf{q}_{2,3} - \mathbf{q}_1$. In the coordinate space the unit vectors are $\mathbf{a}_{1,2} = (4\pi/3k_\theta)(\pm\sqrt{3}/2, 1/2)$. It is useful to introduce complex coordinates $z, \bar{z} = \mathbf{r}_x \pm i\mathbf{r}_y$ in real space and $k, \bar{k} = \mathbf{k}_1 \pm i\mathbf{k}_2$ in momentum space. The Hamiltonian (3) acts on a spinor $\Psi(\mathbf{r}) = (\psi_1, \chi_1, \psi_2, \chi_2, \psi_3, \chi_3)$, where the indices 1,2,3 represent the graphene layer. Introducing the dimensionless twist parameter $\alpha = w_{AB}/(v_F k_\theta)$, and writing the Hamiltonian (3) in the sublattice basis $\Psi(\mathbf{r}) = (\psi_1, \psi_2, \psi_3, \chi_1, \chi_2, \chi_3)$ we obtain

$$\mathcal{H}_{\text{pqTTG}} = \begin{pmatrix} \mathcal{M}(\mathbf{r}) & \mathcal{D}^\dagger(\mathbf{r}) \\ \mathcal{D}(\mathbf{r}) & \mathcal{M}(\mathbf{r}) \end{pmatrix}, \quad (4)$$

where we have rescaled coordinates $\mathbf{r} \rightarrow k_\theta \mathbf{r}$ and the Hamiltonian, so the energies of (4) are measured in units of $v_F k_\theta$. The operators \mathcal{D} and \mathcal{M} are

$$\mathcal{D}(\mathbf{r}) = \begin{pmatrix} -2i\bar{\partial} & \alpha U_1(p\mathbf{r}) & 0 \\ \alpha U_1(-p\mathbf{r}) & -2i\bar{\partial} & \alpha U_1(q(\mathbf{r} - \mathbf{d})) \\ 0 & \alpha U_1(q(\mathbf{d} - \mathbf{r})) & -2i\bar{\partial} \end{pmatrix},$$

$$\mathcal{M}(\mathbf{r}) = \frac{w_{AA}}{w_{AB}} \begin{pmatrix} 0 & U_0(p\mathbf{r}) & 0 \\ U_0(-p\mathbf{r}) & 0 & U_0(q(\mathbf{r} - \mathbf{d})) \\ 0 & U_0(q(\mathbf{d} - \mathbf{r})) & 0 \end{pmatrix}, \quad (5)$$

where $\partial, \bar{\partial} = \frac{1}{2}(\partial_x \mp i\partial_y)$ are complex derivatives and we defined $U_m(\mathbf{r}) = \sum_{n=1}^3 \omega^{m(n-1)} e^{-i\mathbf{q}_n \cdot \mathbf{r}}$ with $\omega = e^{i\phi}$. The Bloch

states $\Psi_{\mathbf{k}}(\mathbf{r}) = (\psi_{\mathbf{k}}(\mathbf{r}), \chi_{\mathbf{k}}(\mathbf{r}))$ of (4) are parametrized by the wave vector \mathbf{k} from mBZ and satisfy the following boundary conditions

$$\Psi_{\mathbf{k}}(\mathbf{r} + \mathbf{a}_{1,2}) = e^{i\mathbf{k} \cdot \mathbf{a}_{1,2}} U_{\phi} \Psi_{\mathbf{k}}(\mathbf{r}), \quad (6)$$

where the matrix $U_{\phi} = \mathbb{1}_{AB} \otimes \text{diag}(\omega^p, 1, \omega^{-q})$.

Below we focus on the chiral limit $w_{AA} = 0$. In this case the Hamiltonian (4) is particle-hole symmetric $\{\mathcal{H}_{\text{pqTTG}}, \sigma_z \otimes 1\} = 0$. The chiral and antichiral zero-energy equations are

$$\mathcal{D}(\mathbf{r})\psi_{\mathbf{k}}(\mathbf{r}) = 0, \quad \mathcal{D}^{\dagger}(\mathbf{r})\chi_{\mathbf{k}}(\mathbf{r}) = 0, \quad (7)$$

and they have solutions for every wave vector \mathbf{k} of the mBZ (flat bands) only at the special values (magic angles) of the twist angle α . We can represent the chiral operator $\mathcal{D}(\mathbf{r})$ in (5) in the form

$$\mathcal{D}(\mathbf{r}) = -2i\bar{\partial} + \alpha\bar{A}(\mathbf{r}), \quad (8)$$

where we introduced the matrix vector-potential $\bar{A}(\mathbf{r})$. The magic angles α can be found numerically as a generalized eigenvalues of the operators $-2i\bar{\partial}$ and $\bar{A}(\mathbf{r})$ [64,65]. Generically the magic angles α form an infinite set of isolated points in the entire complex plane. In order to have magic angles, it is necessary for the chiral operator $\mathcal{D}(\mathbf{r})$ to adhere to specific symmetries. Namely we would like the chiral operator to have three Dirac zero modes ψ_{K_1} , ψ_{K_2} , and ψ_{K_3} at the Dirac points $K_1 = p\mathbf{q}_1$, $K_2 = 0$, and $K_3 = -q\mathbf{q}_1$ for an arbitrary twist angle α . This is guaranteed by C_{3z} symmetry together with the particle-hole symmetry [29,36]. A nonzero displacement \mathbf{d} can break the C_{3z} symmetry of the Hamiltonian. One can show that spectrum of the Hamiltonian (4) is invariant under the following shifts of the displacement

$$\mathbf{d} \rightarrow \mathbf{d} + \frac{1}{pq}\mathbf{a}_{1,2} \quad (9)$$

and the inequivalent displacements that preserve the three Dirac zero modes are $\mathbf{d} = 0$ and $\mathbf{d} = \pm\mathbf{d}_0$, where

$$\mathbf{d}_0 = \frac{1}{3p|q|}(\mathbf{a}_1 - \mathbf{a}_2). \quad (10)$$

The magic angles of the the Hamiltonian are identical for the displacements $\mathbf{d} = \pm\mathbf{d}_0$, because they are related to each other by the $C_{2z}\mathcal{T}$ symmetry, that exchanges the chiral and antichiral components of the Bloch states.

III. ORIGIN OF THE FLAT BANDS

In this section we derive general properties of the zero modes of the Hamiltonian (4) in the chiral limit $w_{AA} = 0$. As we discussed above, the chiral operator admits three Dirac zero modes ψ_{K_1} , ψ_{K_2} and ψ_{K_3} at the Dirac points $K_1 = p\mathbf{q}_1$, $K_2 = 0$, and $K_3 = -q\mathbf{q}_1$

$$\mathcal{D}(\mathbf{r})\psi_{K_i}(\mathbf{r}) = 0, \quad i = 1, 2, 3 \quad (11)$$

for the displacements $\mathbf{d} = 0, \pm\mathbf{d}_0$ and an arbitrary twist angle α . Since the hopping potential has only nonzero off-diagonal elements we get $\text{Tr}\bar{A}(\mathbf{r}) = 0$ and equations (11) one can derive that the Wronskian of the Dirac spinors

$$W(\mathbf{r}) \equiv \det(\psi_{K_1}, \psi_{K_2}, \psi_{K_3}) \quad (12)$$

satisfies $\bar{\partial}W(\mathbf{r}) = 0$ [60,66]. [Note that the Wronskian in this case is simply a triple product, $W(\mathbf{r}) = \psi_{K_1} \cdot (\psi_{K_2} \times \psi_{K_3})$]. Therefore we must conclude that the Wronskian is a constant $W(\mathbf{r}) = W$, since we can not have a nonconstant holomorphic function on a compact manifold, which is a torus in our case.

First we prove that if $W \neq 0$ there is no flat band. $W \neq 0$ implies that $\psi_{K_i}(\mathbf{r})$, $i = 1, 2, 3$ as three-dimensional vectors are linearly independent at each point \mathbf{r} of the moiré unit cell, and form a basis. Therefore any other chiral zero mode $\psi_{\mathbf{k}}(\mathbf{r})$ ($\mathcal{D}\psi_{\mathbf{k}} = 0$) can be expanded as

$$\psi_{\mathbf{k}}(\mathbf{r}) = \mathcal{C}_1(\mathbf{r})\psi_{K_1}(\mathbf{r}) + \mathcal{C}_2(\mathbf{r})\psi_{K_2}(\mathbf{r}) + \mathcal{C}_3(\mathbf{r})\psi_{K_3}(\mathbf{r}),$$

where the scalar functions $\mathcal{C}_{1,2,3}$ must depend on the wave vector \mathbf{k} in order for $\psi_{\mathbf{k}}$ to satisfy the the Bloch boundary conditions (6). Applying the operator $\mathcal{D}(\mathbf{r})$ to both parts of the above equality we conclude that $\bar{\partial}\mathcal{C}_{1,2,3}(\mathbf{r}) = 0$. And since $\psi_{\mathbf{k}}$ and ψ_{K_i} are finite everywhere $\mathcal{C}_i(\mathbf{r})$ can only be constants. But then $\psi_{\mathbf{k}}$ would violate the boundary conditions (6). Therefore if $W \neq 0$ we can not have other zero-energy solutions (and thus flat band) except the Dirac zero modes.

Now, we prove that if $W = 0$, we necessarily have a flat band. $W = 0$ implies that the Dirac spinors $\psi_{K_i}(\mathbf{r})$ as vectors are linearly dependent at every point \mathbf{r} of the moiré unit cell. We stress that it does not mean that they are linearly dependent functions in the Hilbert space. There are two possible scenarios.

Scenario 1. All Bloch spinors of the zero-energy flat bands are collinear at every point \mathbf{r} of the moiré unit cell. We refer to such case as rank 1 flat bands. In this situation any flat band's wave spinor can be described by the following equation:

$$\psi_{\mathbf{k}}(\mathbf{r}) = \mathcal{C}(\mathbf{r})\psi_{K_1}(\mathbf{r}), \quad (13)$$

where $\mathcal{C}(\mathbf{r})$ is some scalar function. If we apply the operator $\mathcal{D}(\mathbf{r})$ to both sides of this equation we obtain $\bar{\partial}\mathcal{C}(\mathbf{r}) = 0$ and thus \mathcal{C} is a constant, which violates the boundary conditions (6) for the spinor $\psi_{\mathbf{k}}$. Therefore Eq. (13) is impossible unless $\psi_{K_1}(\mathbf{r})$ has zeros. If $\psi_{K_1}(\mathbf{r})$ has n zeros at the points \mathbf{r}_{λ} , $\lambda = 1, \dots, n$, we can construct n flat bands, using the following wave functions:

$$\psi_{\mathbf{k}}^{(\lambda)}(\mathbf{r}) = f_{\mathbf{k}-K_1}(z - z_{\lambda})\psi_{K_1}(\mathbf{r}), \quad (14)$$

where $z_{\lambda} = (\mathbf{r}_{\lambda})_x + i(\mathbf{r}_{\lambda})_y$ and we introduced the following meromorphic function:

$$f_{\mathbf{k}}(z) = e^{i\frac{\mathbf{k} \cdot \mathbf{a}_1}{a_1}z} \frac{\vartheta_1(z/a_1 - k/b_2|\omega)}{\vartheta_1(-k/b_2|\omega)\vartheta_1(z/a_1|\omega)}. \quad (15)$$

Normalization of the function $f_{\mathbf{k}}(z)$ is chosen such that $f_{\mathbf{k}+\mathbf{b}_{1,2}}(z) = f_{\mathbf{k}}(z)$ and one can compute that the Chern number of the flat bands in (14) is $C = 1$.

Scenario 2. The other case is that all wave spinors of the flat bands form a two-dimensional vector space at every point \mathbf{r} of the moiré unit cell. We refer to such a case as rank 2 flat bands. In this case we have

$$\psi_{K_3}(\mathbf{r}) = \mathcal{C}_1(\mathbf{r})\psi_{K_1}(\mathbf{r}) + \mathcal{C}_2(\mathbf{r})\psi_{K_2}(\mathbf{r}), \quad (16)$$

where $\mathcal{C}_1(\mathbf{r})$ and $\mathcal{C}_2(\mathbf{r})$ are some scalar functions. If we assume that the spinors $\psi_{K_1}(\mathbf{r})$ and $\psi_{K_2}(\mathbf{r})$ are linearly independent at every point \mathbf{r} of the moiré unit cell and apply the operator $\mathcal{D}(\mathbf{r})$ to both sides of Eq. (16) we obtain $\bar{\partial}\mathcal{C}_{1,2}(\mathbf{r}) = 0$ and thus

$C_{1,2}$ are constants, which violates the boundary conditions (6) for the spinor ψ_{K_3} . Therefore we conclude that there exists at least one point \mathbf{r}_0 where the vectors $\psi_{K_1}(\mathbf{r}_0)$ and $\psi_{K_2}(\mathbf{r}_0)$ are linearly dependent. More generally, there could be n such points \mathbf{r}_λ , $\lambda = 1, \dots, n$, where

$$c_{1\lambda}\psi_{K_1}(\mathbf{r}_\lambda) + c_{2\lambda}\psi_{K_2}(\mathbf{r}_\lambda) = 0, \quad (17)$$

for $\lambda = 1, \dots, n$. [Notice that the coefficients $c_{1,2\lambda}$ are not equal to $C_{1,2}(\mathbf{r}_\lambda)$]. Now it is easy to see that for each zero point \mathbf{r}_λ we can construct a chiral zero mode at every point \mathbf{k} of the mBZ,

$$\begin{aligned} \psi_{\mathbf{k}}^{(\lambda)}(\mathbf{r}) &= (c_{1\lambda}f_{\mathbf{k}-K_1}(z-z_\lambda)\psi_{K_1}(\mathbf{r}) \\ &+ c_{2\lambda}f_{\mathbf{k}-K_2}(z-z_\lambda)\psi_{K_2}(\mathbf{r})). \end{aligned} \quad (18)$$

The function $f_{\mathbf{k}}$ defined in (15) behaves as

$$f_{\mathbf{k}}(z-z_\lambda) \rightarrow \frac{a_1}{\vartheta'_1(0|\omega)} \frac{1}{z-z_\lambda}, \quad z \rightarrow z_\lambda \quad (19)$$

and the poles of the functions $f_{\mathbf{k}-K_1}(z)$ and $f_{\mathbf{k}-K_2}(z)$ are cancelled at the point \mathbf{r}_λ , thus $\psi_{\mathbf{k}}^{(\lambda)}$ is finite at every point of the moiré unit cell. A similar construction within the context of eTTG was proposed by Guerci *et al.* [60].

Since the function $f_{\mathbf{k}}$ in (15) is periodic in the mBZ, but has a pole at $\mathbf{k} = 0$ the function $\psi_{\mathbf{k}}^{(\lambda)}$ can have two poles in mBZ if both coefficients $c_{1\lambda}$ and $c_{2\lambda}$ are not zero. In this case the flat band has the Chern number $C = 2$. If either of the coefficients $c_{1\lambda}$ or $c_{2\lambda}$ is zero, the function $\psi_{\mathbf{k}}^{(\lambda)}$ has one simple pole within the mBZ, we have a rank 1 flat sub-band with the Chern number $C = 1$.

Thus, the rank 2 flat band is characterized by two wave functions $\psi_{K_1}(\mathbf{r})$ and $\psi_{K_2}(\mathbf{r})$. These wave spinors are linearly-independent vectors at every point in the moiré unit cell besides n isolated points \mathbf{r}_λ . Among these points, there may exist n_1 points where either of the spinors ψ_{K_1} or ψ_{K_2} is zero. These points give rise to n_1 flat bands with the Chern number $C = 1$. At the rest of $n_2 = n - n_1$ points ψ_{K_1} and ψ_{K_2} are nonzero and linearly dependent. These points give rise to n_2 flat bands with the Chern number $C = 2$.

We note that the above construction can be easily generalized for the case of twisted ℓ -layer graphene in the chiral limit and shows that one can have flat bands with the Chern number up to $C = \ell - 1$.

Finally we note that we can have only a single Dirac cone on top of the flat bands. To demonstrate this, we observe that if there are two Dirac cones on top of the flat bands, their zero-energy wave spinors must be linearly dependent at some point. Consequently, these wave functions would generate a rank 2 flat band, contradicting the assumption that they constitute distinct zero-energy states.

Below we elaborate more on the possible structures of the flat bands in pqTTG. For this we separately consider cases of $\mathbf{d} = 0$ and $\mathbf{d} = \pm\mathbf{d}_0$ displacements. We summarize all possible configurations of the flat bands in the Figs. 5 and 6.

IV. STRUCTURES OF THE FLAT BANDS

In this section we discuss configurations of the flat bands and their Chern numbers for two different cases of the displacement: $\mathbf{d} = 0$ and $\mathbf{d} = \pm\mathbf{d}_0$.

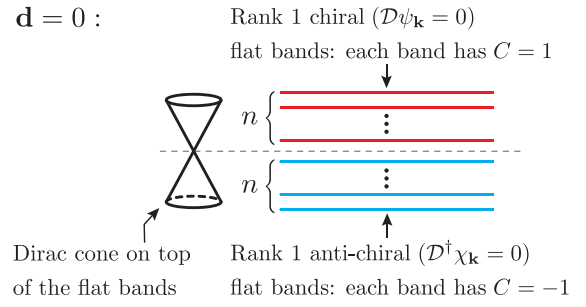


FIG. 5. A structure of the zero-energy flat bands in the case of the displacement $\mathbf{d} = 0$.

A. Displacement $\mathbf{d} = 0$

Absence of the $C = 2$ flat bands. In the case of zero displacement one can construct antichiral zero modes $\chi_{\mathbf{k}}$ ($\mathcal{D}^\dagger \chi_{\mathbf{k}} = 0$) from chiral zero modes $\psi_{\mathbf{k}}$ ($\mathcal{D} \psi_{\mathbf{k}} = 0$) as

$$\begin{aligned} \chi_{\mathbf{k}_{1,2}}(\mathbf{r}) &= Q\bar{\psi}_{\mathbf{k}_{1,2}}(-\mathbf{r}) \\ \chi_{\mathbf{k}}(\mathbf{r}) &= Q(\bar{\psi}_{\mathbf{k}_1}(\mathbf{r}) \times \bar{\psi}_{\mathbf{k}_2}(\mathbf{r})), \end{aligned} \quad (20)$$

where $Q = \text{diag}(1, -1, 1)$, $\mathbf{k} = \mathbf{k}_* - \mathbf{k}_1 - \mathbf{k}_2$ and $\mathbf{k}_* = (p - q)\mathbf{q}_1$. By combining the above formulas we can also construct an additional chiral zero mode $\psi_{\mathbf{k}}$ at the point $\mathbf{k} = \mathbf{k}_* - \mathbf{k}_1 - \mathbf{k}_2$,

$$\psi_{\mathbf{k}}(\mathbf{r}) = \psi_{\mathbf{k}_1}(-\mathbf{r}) \times \psi_{\mathbf{k}_2}(-\mathbf{r}). \quad (21)$$

Moreover one can check that the following function:

$$v(\mathbf{r}) = \psi_{\mathbf{k}_1}(\mathbf{r}) \cdot \psi_{\mathbf{k}_2}(-\mathbf{r}) \quad (22)$$

satisfies $\bar{\partial}v(\mathbf{r}) = 0$ [29], therefore to obey the Bloch boundary conditions v must be zero if $\mathbf{k}_1 \neq \mathbf{k}_2$.

Now let us assume that we have a rank 2 flat band discussed in the *Scenario 2* in the previous section. This means that we have two wave spinors $\psi_{\mathbf{k}_1}$ and $\psi_{\mathbf{k}_2}$ that are linearly independent.

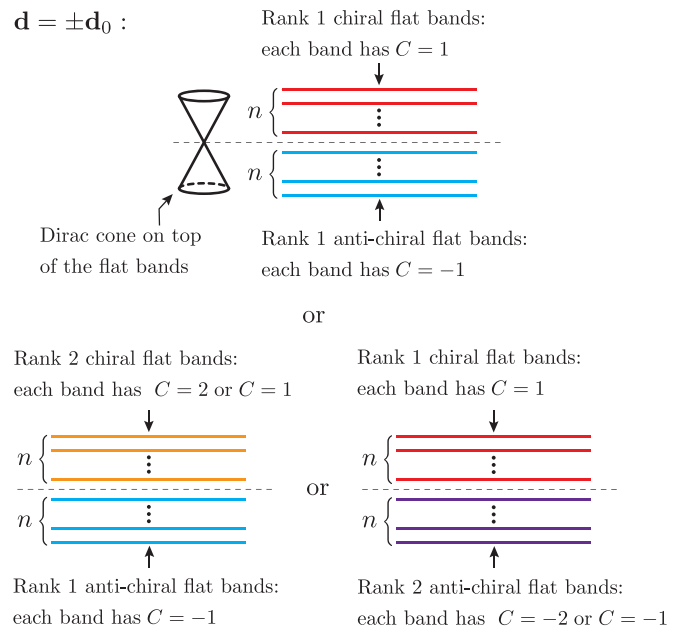


FIG. 6. Possible structures of the zero-energy flat bands in the case of the displacement $\mathbf{d} = \pm\mathbf{d}_0$.

dent as vectors at every point in the moiré unit cell besides n isolated points. By virtue of (21) we have an additional solution $\psi_{\mathbf{k}}$. Let us take a point \mathbf{k}_3 in the mBZ such that $\mathbf{k}_3 \neq \mathbf{k}_{1,2}$, then it is easy to check that

$$\psi_{\mathbf{k}_3} \times \psi_{\mathbf{k}} = \psi_{\mathbf{k}_1}(\psi_{\mathbf{k}_2} \cdot \psi_{\mathbf{k}_3}) - \psi_{\mathbf{k}_2}(\psi_{\mathbf{k}_1} \cdot \psi_{\mathbf{k}_3}) = 0, \quad (23)$$

where we have used that $\psi_{\mathbf{k}_{1,2}} \cdot \psi_{\mathbf{k}_3} = 0$. But it means that $\psi_{\mathbf{k}_3} = \mathcal{C}(\mathbf{r})\psi_{\mathbf{k}}$ for some function $\mathcal{C}(\mathbf{r})$ (two spinors are collinear). Since \mathbf{k}_3 can be arbitrary we conclude that each wave function in the rank 2 flat band is linearly dependent to each other. That is in contradiction with our initial assumption that the flat band has rank 2. Therefore we conclude that for $\mathbf{d} = 0$ the flat bands can not realize *Scenario 2* and thus have the Chern number $C = 2$.

Dirac cone on top of the flat bands. Now we prove that if we have rank 1 flat bands then we must have a Dirac cone on top of them. Namely we prove that we have an additional zero-energy mode of the chiral (and thus also zero-energy mode of the antichiral) operator at an isolated point of the mBZ. We consider a case of a single chiral flat band, when the corresponding wave function $\psi_{\mathbf{k}}(\mathbf{r})$ has only one zero. We can pick such \mathbf{k}_0 for which $\psi_{\mathbf{k}_0}(0) = 0$. Using discussion below (22) one can notice that $\psi_{\mathbf{k}_0}(\mathbf{r}) \cdot \psi_{\mathbf{k}_0}(-\mathbf{r}) = 0$. Due to this fact the following equation:

$$\psi_{\mathbf{k}_0}(\mathbf{r}) = \hat{\phi}_{\mathbf{k}_*-2\mathbf{k}_0}(-\mathbf{r}) \times \psi_{\mathbf{k}_0}(-\mathbf{r}) \quad (24)$$

has a finite solution $\hat{\phi}_{\mathbf{k}_*-2\mathbf{k}_0}$ at the point $\mathbf{k}_* - 2\mathbf{k}_0$ of the mBZ. Then if we apply the operator $\mathcal{D}(\mathbf{r})$ to both sides of this equation we get

$$0 = (\mathcal{D}(-\mathbf{r})\hat{\phi}_{\mathbf{k}_*-2\mathbf{k}_0}(-\mathbf{r})) \times \psi_{\mathbf{k}_0}(-\mathbf{r}), \quad (25)$$

which leads to

$$\mathcal{D}(\mathbf{r})\hat{\phi}_{\mathbf{k}_*-2\mathbf{k}_0}(\mathbf{r}) = \mathcal{C}(\mathbf{r})\psi_{\mathbf{k}_*-2\mathbf{k}_0}(\mathbf{r}). \quad (26)$$

Since $\psi_{\mathbf{k}_*-2\mathbf{k}_0}$ has a zero at some point we can always find a periodic function $g(\mathbf{r})$ [66] such that

$$(\mathcal{C}(\mathbf{r}) + \bar{\partial}g(\mathbf{r}))\psi_{\mathbf{k}_*-2\mathbf{k}_0}(\mathbf{r}) = 0 \quad (27)$$

and therefore we can construct a solution $\phi_{\mathbf{k}_*-2\mathbf{k}_0}(\mathbf{r}) = \hat{\phi}_{\mathbf{k}_*-2\mathbf{k}_0}(\mathbf{r}) + g(\mathbf{r})\psi_{\mathbf{k}_*-2\mathbf{k}_0}(\mathbf{r})$ that belongs to a specific point of the mBZ and satisfies the equation

$$\mathcal{D}(\mathbf{r})\phi_{\mathbf{k}_*-2\mathbf{k}_0}(\mathbf{r}) = 0. \quad (28)$$

This concludes the classification of the flat bands structures for $\mathbf{d} = 0$. In summary, we can have only chiral and antichiral flat bands of rank 1 with the Chern numbers $C = 1$ and $C = -1$ with a single Dirac cone on top of them. This is schematically depicted in Fig. 5.

B. Displacement $\mathbf{d} = \pm\mathbf{d}_0$

Possible topologies of the flat bands. In the case of nonzero displacement $\mathbf{d} = \pm\mathbf{d}_0$ we can construct an antichiral zero mode by taking cross product of two chiral zero modes,

$$\chi_{\mathbf{k}_s-\mathbf{k}_1-\mathbf{k}_2}(\mathbf{r}) = Q(\bar{\psi}_{\mathbf{k}_1}(\mathbf{r}) \times \bar{\psi}_{\mathbf{k}_2}(\mathbf{r})). \quad (29)$$

Even though we can not construct an antichiral mode from a chiral one using complex conjugation and inversion as in (20), the number of antichiral flat bands must be equal to the number of the chiral ones, because of the particle-hole symmetry.

Also similarly to the $\mathbf{d} = 0$ case one can show that the following function:

$$v(\mathbf{r}) = \bar{\chi}_{\mathbf{k}_1}(-\mathbf{r})Q\psi_{\mathbf{k}_2}(\mathbf{r}) \quad (30)$$

satisfies $\bar{\partial}v(\mathbf{r}) = 0$ and thus is equal to zero if $\mathbf{k}_1 \neq \mathbf{k}_2$.

Unlike the case $\mathbf{d} = 0$, when $\mathbf{d} = \pm\mathbf{d}_0$ there are no obstacles preventing the existence of rank 2 flat bands. Let us assume that we have a rank 2 chiral flat band, thus we have two linearly independent (besides n points) wave spinors $\psi_{\mathbf{k}_1}$ and $\psi_{\mathbf{k}_2}$. Using (29) we construct an antichiral zero mode $\chi_{\mathbf{k}}$. The number of zeros of $\chi_{\mathbf{k}}$ is equal to the number of points where $\psi_{\mathbf{k}_1}$ and $\psi_{\mathbf{k}_2}$ are linearly dependent. If we assume that there is some other antichiral zero mode $\chi_{\mathbf{k}_3}$ with $\mathbf{k}_3 \neq \mathbf{k}_1, \mathbf{k}_2$ we have

$$\chi_{\mathbf{k}}(\mathbf{r}) \times \chi_{\mathbf{k}_3}(\mathbf{r}) = Q(Q(\psi_{\mathbf{k}_1} \times \psi_{\mathbf{k}_2}) \times \bar{\chi}_{\mathbf{k}_3}) = 0, \quad (31)$$

where we used (30). Therefore the antichiral flat band must have rank 1. From that it follows that we can not have at the same time rank 2 chiral and antichiral flat bands. Also one can prove that the Dirac cone on top of the flat bands is prohibited in this case.

Finally, if we assume that we have a rank 1 chiral flat band $\psi_{\mathbf{k}}$ and one Dirac cone on top of it with its zero mode $\phi_{\mathbf{k}_0}$. Then using (29) for $\phi_{\mathbf{k}_0}$ and $\psi_{\mathbf{k}}$ we can construct a rank 1 antichiral flat band. And vice versa, using the same argument as in the previous subsection we can prove that if we have rank 1 chiral and antichiral flat bands, we must have a single Dirac cone on top of them. We show schematically in Fig. 6 all the possible cases for $\mathbf{d} = \pm\mathbf{d}_0$.

ACKNOWLEDGMENTS

We are grateful to Simon Becker, Tristan Humbert, Igor R. Klebanov, Jens Wittsten, and Mengxuan Yang for useful discussions. We would like to thank Igor R. Klebanov for valuable comments on the draft. F.K.P. is currently a Simons Junior Fellow at New York University and supported by Grant No. 855325FP from the Simons Foundation.

- [1] R. Bistritzer and A. H. MacDonald, Moiré bands in twisted double-layer graphene, *Proc. Natl. Acad. Sci. USA* **108**, 12233 (2011).
- [2] E. Suárez Morell, J. D. Correa, P. Vargas, M. Pacheco, and Z. Barticevic, Flat bands in slightly twisted bilayer graphene: Tight-binding calculations, *Phys. Rev. B* **82**, 121407(R) (2010).

- [3] Y. Cao, V. Fatemi, S. Fang, K. Watanabe, T. Taniguchi, E. Kaxiras, and P. Jarillo-Herrero, Unconventional superconductivity in magic-angle graphene superlattices, *Nature (London)* **556**, 43 (2018).
- [4] Y. Cao, V. Fatemi, A. Demir, S. Fang, S. L. Tomarken, J. Y. Luo, J. D. Sanchez-Yamagishi, K. Watanabe, T. Taniguchi, E. Kaxiras *et al.*, Correlated insulator behaviour at half-filling in

- magic-angle graphene superlattices, *Nature (London)* **556**, 80 (2018).
- [5] M. Yankowitz, S. Chen, H. Polshyn, Y. Zhang, K. Watanabe, T. Taniguchi, D. Graf, A. F. Young, and C. R. Dean, Tuning superconductivity in twisted bilayer graphene, *Science* **363**, 1059 (2019).
 - [6] H. C. Po, L. Zou, A. Vishwanath, and T. Senthil, Origin of mott insulating behavior and superconductivity in twisted bilayer graphene, *Phys. Rev. X* **8**, 031089 (2018).
 - [7] A. Thomson, S. Chatterjee, S. Sachdev, and M. S. Scheurer, Triangular antiferromagnetism on the honeycomb lattice of twisted bilayer graphene, *Phys. Rev. B* **98**, 075109 (2018).
 - [8] L. Zou, H. C. Po, A. Vishwanath, and T. Senthil, Band structure of twisted bilayer graphene: Emergent symmetries, commensurate approximants, and Wannier obstructions, *Phys. Rev. B* **98**, 085435 (2018).
 - [9] F. Guinea and N. R. Walet, Electrostatic effects, band distortions, and superconductivity in twisted graphene bilayers, *Proc. Natl. Acad. Sci. USA* **115**, 13174 (2018).
 - [10] S. Carr, S. Fang, P. Jarillo-Herrero, and E. Kaxiras, Pressure dependence of the magic twist angle in graphene superlattices, *Phys. Rev. B* **98**, 085144 (2018).
 - [11] Y. Su and S.-Z. Lin, Pairing symmetry and spontaneous vortex-antivortex lattice in superconducting twisted-bilayer graphene: Bogoliubov-de Gennes approach, *Phys. Rev. B* **98**, 195101 (2018).
 - [12] J. González and T. Stauber, Kohn-Luttinger superconductivity in twisted bilayer graphene, *Phys. Rev. Lett.* **122**, 026801 (2019).
 - [13] F. Wu, T. Lovorn, E. Tutuc, I. Martin, and A. H. MacDonald, Topological insulators in twisted transition metal dichalcogenide homobilayers, *Phys. Rev. Lett.* **122**, 086402 (2019).
 - [14] D. K. Efimkin and A. H. MacDonald, Helical network model for twisted bilayer graphene, *Phys. Rev. B* **98**, 035404 (2018).
 - [15] N. F. Q. Yuan and L. Fu, Model for the metal-insulator transition in graphene superlattices and beyond, *Phys. Rev. B* **98**, 045103 (2018).
 - [16] C. Xu and L. Balents, Topological superconductivity in twisted multilayer graphene, *Phys. Rev. Lett.* **121**, 087001 (2018).
 - [17] M. Ochi, M. Koshino, and K. Kuroki, Possible correlated insulating states in magic-angle twisted bilayer graphene under strongly competing interactions, *Phys. Rev. B* **98**, 081102(R) (2018).
 - [18] F. Wu, A. H. MacDonald, and I. Martin, Theory of phonon-mediated superconductivity in twisted bilayer graphene, *Phys. Rev. Lett.* **121**, 257001 (2018).
 - [19] Y.-H. Zhang, D. Mao, Y. Cao, P. Jarillo-Herrero, and T. Senthil, Nearly flat Chern bands in moiré superlattices, *Phys. Rev. B* **99**, 075127 (2019).
 - [20] J. Kang and O. Vafek, Symmetry, maximally localized wannier states, and a low-energy model for twisted bilayer graphene narrow bands, *Phys. Rev. X* **8**, 031088 (2018).
 - [21] J. M. Pizarro, M. J. Calderón, and E. Bascones, The nature of correlations in the insulating states of twisted bilayer graphene, *J. Phys. Commun.* **3**, 035024 (2019).
 - [22] M. Koshino, N. F. Q. Yuan, T. Koretsune, M. Ochi, K. Kuroki, and L. Fu, Maximally localized Wannier orbitals and the extended Hubbard model for twisted bilayer graphene, *Phys. Rev. X* **8**, 031087 (2018).
 - [23] D. M. Kennes, J. Lischner, and C. Karrasch, Strong correlations and $d + id$ superconductivity in twisted bilayer graphene, *Phys. Rev. B* **98**, 241407(R) (2018).
 - [24] H. Isobe, N. F. Q. Yuan, and L. Fu, Unconventional superconductivity and density waves in twisted bilayer graphene, *Phys. Rev. X* **8**, 041041 (2018).
 - [25] L. Rademaker and P. Mellado, Charge-transfer insulation in twisted bilayer graphene, *Phys. Rev. B* **98**, 235158 (2018).
 - [26] T. J. Peltonen, R. Ojajärvi, and T. T. Heikkilä, Mean-field theory for superconductivity in twisted bilayer graphene, *Phys. Rev. B* **98**, 220504(R) (2018).
 - [27] V. Kozii, H. Isobe, J. W. F. Venderbos, and L. Fu, Nematic superconductivity stabilized by density wave fluctuations: Possible application to twisted bilayer graphene, *Phys. Rev. B* **99**, 144507 (2019).
 - [28] V. Kozii, M. P. Zaletel, and N. Bultinck, Spin-triplet superconductivity from intervalley goldstone modes in magic-angle graphene, *Phys. Rev. B* **106**, 235157 (2022).
 - [29] G. Tarnopolsky, A. J. Kruchkov, and A. Vishwanath, Origin of magic angles in twisted bilayer graphene, *Phys. Rev. Lett.* **122**, 106405 (2019).
 - [30] P. San-Jose, J. González, and F. Guinea, Non-Abelian gauge potentials in graphene bilayers, *Phys. Rev. Lett.* **108**, 216802 (2012).
 - [31] Z. Song, Z. Wang, W. Shi, G. Li, C. Fang, and B. A. Bernevig, All magic angles in twisted bilayer graphene are topological, *Phys. Rev. Lett.* **123**, 036401 (2019).
 - [32] K. Hejazi, C. Liu, H. Shapourian, X. Chen, and L. Balents, Multiple topological transitions in twisted bilayer graphene near the first magic angle, *Phys. Rev. B* **99**, 035111 (2019).
 - [33] H. C. Po, L. Zou, T. Senthil, and A. Vishwanath, Faithful tight-binding models and fragile topology of magic-angle bilayer graphene, *Phys. Rev. B* **99**, 195455 (2019).
 - [34] Y. Sheffer, R. Queiroz, and A. Stern, Symmetries as the guiding principle for flattening bands of Dirac fermions, *Phys. Rev. X* **13**, 021012 (2023).
 - [35] E. Khalaf, A. J. Kruchkov, G. Tarnopolsky, and A. Vishwanath, Magic angle hierarchy in twisted graphene multilayers, *Phys. Rev. B* **100**, 085109 (2019).
 - [36] C. Mora, N. Regnault, and B. A. Bernevig, Flatbands and perfect metal in trilayer moiré graphene, *Phys. Rev. Lett.* **123**, 026402 (2019).
 - [37] T. Cea, N. R. Walet, and F. Guinea, Twists and the electronic structure of graphitic materials, *Nano Lett.* **19**, 8683 (2019).
 - [38] Z. Zhu, S. Carr, D. Massatt, M. Luskin, and E. Kaxiras, Twisted trilayer graphene: A precisely tunable platform for correlated electrons, *Phys. Rev. Lett.* **125**, 116404 (2020).
 - [39] Y. Mao, D. Guerzi, and C. Mora, Supermoiré low-energy effective theory of twisted trilayer graphene, *Phys. Rev. B* **107**, 125423 (2023).
 - [40] X. Lin, C. Li, K. Su, and J. Ni, Energetic stability and spatial inhomogeneity in the local electronic structure of relaxed twisted trilayer graphene, *Phys. Rev. B* **106**, 075423 (2022).
 - [41] Z. Ma, S. Li, M. Lu, D.-H. Xu, J.-H. Gao, and X. Xie, Doubled moiré flat bands in double-twisted few-layer graphite, *Sci. China Phys. Mech. Astron.* **66**, 227211 (2023).
 - [42] M. Liang, M.-M. Xiao, Z. Ma, and J.-H. Gao, Moiré band structures of the double twisted few-layer graphene, *Phys. Rev. B* **105**, 195422 (2022).

- [43] J. Y. Lee, E. Khalaf, S. Liu, X. Liu, Z. Hao, P. Kim, and A. Vishwanath, Theory of correlated insulating behaviour and spin-triplet superconductivity in twisted double bilayer graphene, *Nat. Commun.* **10**, 5333 (2019).
- [44] P. J. Ledwith, A. Vishwanath, and E. Khalaf, Family of ideal Chern flatbands with arbitrary Chern number in chiral twisted graphene multilayers, *Phys. Rev. Lett.* **128**, 176404 (2022).
- [45] P. J. Ledwith, E. Khalaf, Z. Zhu, S. Carr, E. Kaxiras, and A. Vishwanath, TB or not TB? Contrasting properties of twisted bilayer graphene and the alternating twist n -layer structures ($n = 3, 4, 5, \dots$), [arXiv:2111.11060](https://arxiv.org/abs/2111.11060).
- [46] J. Wang and Z. Liu, Hierarchy of ideal flatbands in chiral twisted multilayer graphene models, *Phys. Rev. Lett.* **128**, 176403 (2022).
- [47] S. Zhang, B. Xie, Q. Wu, J. Liu, and O. V. Yazyev, Chiral decomposition of twisted graphene multilayers with arbitrary stacking, *Nano Lett.* **23**, 2921 (2023).
- [48] M. Yang, Flat bands and high Chern numbers in twisted multilayer graphene, [arXiv:2303.00103](https://arxiv.org/abs/2303.00103).
- [49] X. Zhang, K.-T. Tsai, Z. Zhu, W. Ren, Y. Luo, S. Carr, M. Lusk, E. Kaxiras, and K. Wang, Correlated insulating states and transport signature of superconductivity in twisted trilayer graphene superlattices, *Phys. Rev. Lett.* **127**, 166802 (2021).
- [50] J. M. Park, Y. Cao, K. Watanabe, T. Taniguchi, and P. Jarillo-Herrero, Tunable strongly coupled superconductivity in magic-angle twisted trilayer graphene, *Nature (London)* **590**, 249 (2021).
- [51] Z. Hao, A. M. Zimmerman, P. Ledwith, E. Khalaf, D. H. Najafabadi, K. Watanabe, T. Taniguchi, A. Vishwanath, and P. Kim, Electric field-tunable superconductivity in alternating-twist magic-angle trilayer graphene, *Science* **371**, 1133 (2021).
- [52] X. Liu, N. J. Zhang, K. Watanabe, T. Taniguchi, and J. I. A. Li, Isospin order in superconducting magic-angle twisted trilayer graphene, *Nat. Phys.* **18**, 522 (2022).
- [53] S. Turkel, J. Swann, Z. Zhu, M. Christos, K. Watanabe, T. Taniguchi, S. Sachdev, M. S. Scheurer, E. Kaxiras, C. R. Dean, and A. N. Pasupathy, Orderly disorder in magic-angle twisted trilayer graphene, *Science* **376**, 193 (2022).
- [54] A. Uri, S. C. de la Barrera, M. T. Randeria, D. Rodan-Legrain, T. Devakul, P. J. D. Crowley, N. Paul, K. Watanabe, T. Taniguchi, R. Lifshitz *et al.*, Superconductivity and strong interactions in a tunable moiré quasiperiodic crystal, *Nature (London)* **620**, 762 (2023).
- [55] D. Călugăru, F. Xie, Z.-D. Song, B. Lian, N. Regnault, and B. A. Bernevig, Twisted symmetric trilayer graphene: Single-particle and many-body Hamiltonians and hidden nonlocal symmetries of trilayer moiré systems with and without displacement field, *Phys. Rev. B* **103**, 195411 (2021).
- [56] F. Xie, N. Regnault, D. Călugăru, B. A. Bernevig, and B. Lian, Twisted symmetric trilayer graphene. II. Projected Hartree-Fock study, *Phys. Rev. B* **104**, 115167 (2021).
- [57] M. Christos, S. Sachdev, and M. S. Scheurer, Correlated insulators, semimetals, and superconductivity in twisted trilayer graphene, *Phys. Rev. X* **12**, 021018 (2022).
- [58] F. K. Popov and G. Tarnopolsky, Magic angles in equal-twist trilayer graphene, *Phys. Rev. B* **108**, L081124 (2023).
- [59] D. C. W. Foo, Z. Zhan, Mohammed M. Al. Ezzi, L. Peng, S. Adam, and F. Guinea, Extended magic phase in twisted graphene multilayers, [arXiv:2305.18080](https://arxiv.org/abs/2305.18080).
- [60] D. Guerci, Y. Mao, and C. Mora, Chern mosaic and ideal flat bands in equal-twist trilayer graphene, [arXiv:2305.03702](https://arxiv.org/abs/2305.03702).
- [61] T. Devakul, P. J. Ledwith, L.-Q. Xia, A. Uri, S. de la Barrera, P. Jarillo-Herrero, and L. Fu, Magic-angle helical trilayer graphene, *Sci. Adv.* **9**, adi6063 (2023).
- [62] N. Nakatsuji, T. Kawakami, and M. Koshino, Multi-scale lattice relaxation in chiral twisted trilayer graphenes, [arXiv:2305.13155](https://arxiv.org/abs/2305.13155).
- [63] J. Kang and O. Vafek, Pseudomagnetic fields, particle-hole asymmetry, and microscopic effective continuum Hamiltonians of twisted bilayer graphene, *Phys. Rev. B* **107**, 075408 (2023).
- [64] S. Becker, M. Embree, J. Wittsten, and M. Zworski, Spectral characterization of magic angles in twisted bilayer graphene, *Phys. Rev. B* **103**, 165113 (2021).
- [65] S. Becker, M. Embree, J. Wittsten, and M. Zworski, Mathematics of magic angles in a model of twisted bilayer graphene, *Prob. Math. Phys.* **3**, 69 (2022).
- [66] F. K. Popov and A. Milekhin, Hidden wave function of twisted bilayer graphene: The flat band as a Landau level, *Phys. Rev. B* **103**, 155150 (2021).